Phys. Solid State 7, 2032 (1966)].
[2]H. Koehler and Z. Angew, Phys. 23, 270 (1967).
[3]L. M. Rogers, J. Phys. D 1, 845 (1968).
[4]R. Tsu, W. E. Howard, and L. Esaki, Phys. Rev. 172, 779 (1968).
[5]H. R. Riedl, J. R. Dixon, and R. B. Schoolar, Phys. Rev. 162, 692 (1967).
[6]B. B. Houston, R. F. Bis, and E. Gubner, Bull. Am. Phys. Soc. 6, 436 (1961).
[7]R. F. Brebrick, J. Phys. Chem. Solids 24, 27 (1963).
[8]B. B. Houston, R. S. Allgaier, J. Babiskin, and P. G. Siebenmann, Bull. Am. Phys. Soc. 9, 60 (1964).
[9]M. K. Norr, J. Electrochem. Soc. 113, 621 (1966).
[10]R. F. Bis, Ph. D. thesis, University of Maryland, 1969 (unpublished).
[11]H. R. Riedl, R. B. Schoolar, and B. B. Houston, Solid State Commun. 4, 399 (1966).
[12]F. Stern, in *Solid State Physics*, edited by F. Seitz and D. Turnbull (Academic, New York, 1963), Vol. 15, p. 344.
[13]R. B. Schoolar, H. R. Riedl, and J. R. Dixon, Solid State Commun. 4, 423 (1966).
[14]R. B. Schoolar and J. R. Dixon, J. Opt. Soc. Am. 58, 119 (1968).
[15]H. R. Riedl and R. B. Schoolar, Phys. Rev. 131, 2082 (1963).
[16]Thickness of sample *F* was obtained by private communication with R. B. Schoolar, U.S. Naval Ordnance Lab.
[17]E. Burstein, Phys. Rev. 93, 632 (1954).
[18]J. R. Dixon and H. R. Riedl, Phys. Rev. 138, 873 (1965).
[19]J. N. Zemel, J. D. Jensen, and R. B. Schoolar, Phys. Rev. 140, A330 (1965).
[20]B. B. Houston and R. S. Allgaier, Bull. Am. Phys. Soc. 9, 293 (1964).
[21]M. H. Cohen, Phys. Rev. 121, 387 (1961).
[22]R. S. Allgaier, Phys. Rev. 152, 808 (1966).
[23]L. Esaki and P. J. Stiles, Phys. Rev. Letters 16, 1108 (1966).
[24]Experimental results reported for GeTe (Ref. 4) suggest the possibility that such an anomaly may exist in this material. However, the evidence is not as clear cut as in the case of SnTe, since the variations of the mass with temperature are considerably smaller and are nonuniform with carrier concentration.
[25]J. R. Burke and H. R. Riedl, Phys. Rev. 184, 830 (1969).

PHYSICAL REVIEW B VOLUME 2, NUMBER 4 15 AUGUST 1970

Electron Mobility in Direct-Gap Polar Semiconductors

D. L. Rode
Bell Telephone Laboratories, Murray Hill, New Jersey
(Received 30 March 1970)

The electron drift mobilities of the five direct-gap III-V semiconductors GaAs, GaSb, InP, InAs, and InSb are presented as a function of temperature. Polar-mode, deformation-potential acoustic, and piezoelectric scattering are included, as well as nonparabolic conduction bands and the corresponding electron wave functions. The drift mobility follows exactly from the assumed model by a simple iterative technique of solution which retains all the advantages of variational techniques without, however, the need for excessive mathematical detail. Piezoelectric scattering is shown to be considerable in GaAs for temperatures below 100 °K. The agreement between theory and experiment for GaAs is satisfactory.

I. INTRODUCTION

In recent years, considerable interest has developed toward the study[1,2] and use[3,4] of compound semiconductors. The materials about which the most detailed information is available possess direct energy gaps and are derived from elements in columns III and V of the Periodic Table. These semiconductors are five in number: GaAs, GaSb, InP, InAs, and InSb.

Compound semiconductors are peculiarly useful because electron transport at high (but easily achieved) electric fields is dominated by the complex conduction-band structure well above the lowest band edge.[5,6] Devices relying on the influence of the higher-energy areas of the conduction band represent a new class of applications (e.g., bulk effects[7,8]) distinct from that involving energies within a few times the thermal energy of the band edge. Obviously, one now has a wider selection of band structures available, as compared to column-IV semiconductors alone. In addition, the five semiconductors listed above have exhibited some of the highest electron mobilities attained in the liquid-nitrogen to room-temperature range. Hall effect detector devices, of course, operate more efficiently with high mobilities.

The electron mobility is a popular parameter

used to characterize the microscopic quality of crystals. Accurate comparisons between experiment and theory are important for determining a variety of fundamental material constants and electron scattering mechanisms through which high-field transport properties can be calculated.[5] This procedure ultimately exposes potential areas of device applications.

Having reviewed some advantages of compound semiconductors, we now state the purpose of the present paper and briefly review the status of mobility calculations (see also the review by Blatt[9]).

The purpose of this paper is to present calculations of the electron mobility in direct-gap polar semiconductors. In particular, the calculations are exact once the fairly accurate model (described below) of the material is assumed. Results are presented for *pure* III-V semiconductors. The method of calculating the mobility relies on the fact that a great deal of analytical progress can be achieved regarding the scattering terms of the Boltzmann equation. An explicit expression for the electron distribution function perturbed by a small electric field is obtained as a linear finite difference equation. Several scattering mechanisms are properly combined, and the mobility is calculated from the perturbed distribution.

Two types of scattering have been previously shown by Ehrenreich[10] to be operative in the (000) valley of pure nondegenerate semiconductors: acoustic-mode scattering through the deformation-potential interaction,[11] and polar-optical-mode scattering.[12,13] There is, however, the additional possibility of piezoelectric scattering,[14,15] which has been included here. This type of scattering is also attributable to acoustic modes, but the interaction takes place through piezoelectric coupling to longitudinal electric fields.[16,17] In fact, it turns out that piezoelectric scattering is the most important mode of scattering for lattice temperatures T below about 60 °K in GaAs. It becomes noticeable at 100 to 150 °K, below which it is more effective than deformation-potential scattering. Thus, the present model includes all three of the above types of electron scattering. Furthermore, the various scattering mechanisms are properly combined *before* the perturbed electron distribution function is calculated so that Matthiessen's rule is not invoked.[18]

Before scattering effects can be calculated, a model for the conduction band must be assumed. Kane[19] has accurately determined the structure of the lowest (000) conduction-band minimum at the center of the first Brillouin zone as well as the electron wave functions in this valley. The band structure results from a simultaneous diagonalization of the conduction–valence-band $\vec{k}\cdot\vec{p}$ interaction Hamiltonian and the atomic spin-orbit interaction Hamiltonian. Electrons at the conduction-band edge (where the crystal momentum $\hbar\vec{k}$ vanishes) possess wave functions having the symmetry properties of s functions with respect to the tetrahedral group operations. This is to be expected since these electrons are nonlocalized and are then described by plane waves. At energies above the band edge, the electrons become more localized so they are able to sense the orbital p states of the lattice (and atomic spin-orbit coupling) for at least a small average part of their motion (see, for example, Slater[20]). The electron wave function is then given by Kane as a linear combination of s and p functions. The dependence of electron energy upon crystal momentum is no longer parabolic. Regarding transport properties, both the band nonparabolicity and the functional dependence of the wave function upon crystal momentum are about equally important. Hence, the two effects are treated here simultaneously in a self-consistent fashion.

Mobility has, in the past, been calculated by relaxation time and variational methods,[21] the particular method being dictated by scattering mechanisms.[22] When the scattering mechanism is elastic, a relaxation time characterizing the rate at which momentum decays can be defined. From the relaxation time, one can calculate the perturbation of an equilibrium electron distribution by a small electric field and, hence, the mobility. When the scattering is inelastic, no relaxation time exists exactly, although in certain limits this approximation can be useful. Actually, for much of the temperature range of interest the relaxation-time concept must be abandoned because of the dominance of inelastic scattering. The resulting problem has previously been solved by variational calculations[23] in this latter circumstance. Specifically, the failure of the relaxation-time concept forces one into a variational approach.

The present mobility calculation includes the three types of electron scattering mentioned earlier: (i) acoustic-mode deformation-potential coupling, (ii) acoustic-mode piezoelectric coupling, and (iii) polar-optical-mode polarization coupling. The first two are elastic processes while the latter is inelastic. Howarth and Sondheimer[24] have achieved an analytical reduction of polar-mode scattering [case (iii) above] in the Boltzmann equation assuming a spherical and parabolic conduction-band valley. They apply the results to a variational calculation proposed by Kohler[21] and determine the mobility. Ehrenreich[25,26] improved these calculations by including Kane's[19] picture of the conduction band and by including other types of scattering in a variational calculation.

With an accurate model of the band structure and electron wave functions available,[19] an exact mobility calculation based upon this picture is in order. The present method avoids much of the purely mathematical detail necessary for the variational method. The procedure is straightforward enough so that the physics of the results are clear; and, in fact, we will find that all of the advantages of the variational approach are preserved. These include estimating the algebraic sign and the magnitude of corrections to approximate solutions as well as the total avoidance of Matthiessen's rule.[9] One obtains a linear finite difference equation, as previously,[24, 26] which describes the electron distribution function under the influence of a small electric field. The equation is solved by numerical iteration rather than by the method of Grigor'ev *et al.*,[27] who applied a numerical method to a simpler band-structure model of InSb.

The mobility calculated here includes the three most significant types of scattering, mentioned earlier, in *pure* nondegenerate materials and is accurate for the following temperature ranges: for GaAs ~ 2–500 °K, for GaSb ~2–170 °K, for InP ~2–600 °K, for InAs ~2–400 °K, for InSb ~2–250 °K. The absolute error above 60 °K may be near 15%, the larger part of which results from uncertainty in the high- and low-frequency dielectric constants and electron effective mass. Below 100 °K, the error may be as large as 30%, reflecting some doubt about the piezoelectric constants and acoustic deformation potentials.

In Sec. II, the conduction-band model and electron wave functions from Kane's work[19] are adapted to the present calculation. The electron distribution function is presented formally in Sec. III along with a spherical harmonic decomposition of the Boltzmann equation. In Sec. IV, various scattering mechanisms are discussed and cast into a form suitable for substitution into the Boltzmann equation. The electron distribution function in the presence of a small electric field is determined explicitly in Sec. V. Material parameters and calculated mobilities are presented in Sec. VI.

II. BAND STRUCTURE AND WAVE FUNCTIONS

The dispersion relation for energy $\mathcal{E}$ measured upward from the conduction-band edge at $\vec{k} = (0, 0, 0)$ is given by Kane[19]:

$$(\mathcal{E}-\mathcal{E}_0)(\mathcal{E}-\mathcal{E}_0+\mathcal{E}_g)(\mathcal{E}-\mathcal{E}_0+\mathcal{E}_g+\Delta) - \mathcal{E}_0\mathcal{E}_p(\mathcal{E}-\mathcal{E}_0+\mathcal{E}_g+\tfrac{2}{3}\Delta)=0\,. \quad (1)$$

$\mathcal{E}_g$ is the effective-mass energy gap as discussed by Ehrenrich,[26] Δ is the spin-orbit splitting of the valence band, and

$$\mathcal{E}_0=\hbar^2\vec{k}^2/2m\,, \quad (2)$$

where m is the free-electron mass. $\mathcal{E}_p$ characterizes the strength of the conduction-band–valence-band coupling. The cubic [Eq. (1)] can be reduced to an expression quadratic in energy if the spin-orbit splitting is neglected. In fact, we assume that $\Delta = 0$. This approximation is as accurate as Eq. (1) to the following errors in energy: (a) for $\mathcal{E} \leq \frac{1}{2}\mathcal{E}_g$, error $\lesssim 4.2\%$ (maximum error at $\Delta^2 = \frac{9}{4}\mathcal{E}_g^2$), (b) for $\mathcal{E} \leq \frac{1}{4}\mathcal{E}_g$, error $\lesssim 2.3\%$ (maximum error at $\Delta^2 = \frac{15}{8}\mathcal{E}_g^2$). In particular, the actual error in GaAs is about half these maximum values since Δ is rather small[10] ($\Delta \approx 0.22\,\mathcal{E}_g$). For accuracy beyond a few percent one must include the influence of higher-lying conduction-band valleys anyway. Hence, the energy is to be taken from Eq. (1) with $\Delta = 0$:

$$\mathcal{E} = \mathcal{E}_0 + (\alpha - 1)\tfrac{1}{2}\mathcal{E}_g\,, \quad (3)$$

where

$$\alpha^2 = 1 + 4\mathcal{E}_0(m-m^*)/m^*\mathcal{E}_g \quad (4)$$

and m^* is the electron effective mass at the conduction-band edge.

The quantity α is greater than or equal to (at $k = 0$) unity, and for small energies Eq. (3) simply yields the parabolic relation between energy and crystal momentum, $\mathcal{E} = \hbar^2\vec{k}^2/2m^*$. Equations (3) and (4) describe a subparabolic $\mathcal{E}$-versus-k relation. The density-of-states function in energy space must therefore be superlinear versus k. Equivalently, one can regard the effective mass as a weakly increasing function of crystal momentum. This augmented density of states, relative to that for a parabolic band, which we shall denote as d will appear again later in relation to electron scattering rates (Sec. IV):

$$\frac{1}{d} = m\,\frac{\partial\mathcal{E}}{\partial k}\Big/\hbar^2 k. \quad (5)$$

From Eq. (3),

$$1/d = 1 + (m-m^*)/m^*\alpha, \quad (6)$$

where α is defined by Eq. (4). When the crystal momentum vanishes $m\cdot d = m^*$.

The transition rate between two electron states with crystal momenta $\hbar\vec{k}$ and $\hbar\vec{k}'$ is directly proportional to the absolute square of the overlap integral of the respective wave functions.[26] In the present band picture, the electron wave function $\varphi_{c\alpha}$ is constructed from an s function and a p function, the major part of $\varphi_{c\alpha}$ being of type s. The small p-function admixture accounts for the electron interaction with the light-mass and split-off valence bands which, of course, are now degenerate at $k = 0$ since $\Delta = 0$. For one spin direction α,[19]

$$\varphi_{c\alpha} = a[iS\downarrow]' + c[Z\downarrow]'\,, \quad (7)$$

where $|iS\downarrow\rangle$ and $|Z\downarrow\rangle$ are basis functions with $\downarrow$

meaning spin up and ↓ meaning spin down and primes denoting coordinate and spin transformations. The real coefficients a and c are non-negative functions of crystal momentum [see Eq. (4)]. These coefficients follow simply in the $\Delta = 0$ approximation which again represents the scattering rate accurately to within a few percent:

$$2a^2 = 1 + 1/\alpha, \tag{8}$$

$$a^2 + c^2 = 1. \tag{9}$$

When the crystal momentum approaches zero, $a \to 1$ and $c \to 0$. These coefficients provide the absolute square of the overlap integral $G(\vec{k}, \vec{k}')$ in terms of band parameters and the crystal momenta before and after scattering, $\hbar\vec{k}$ and $\hbar\vec{k}'$, respectively. Applying Matz's results[28] with $\Delta = 0$, we have

$$G(\vec{k}, \vec{k}') = (aa' + cc'x)^2, \tag{10}$$

where x equals the cosine of the angle between $\vec{k}$ and $\vec{k}'$, and (a, c) are evaluated at $\vec{k}$ while (a', c') are evaluated at $\vec{k}'$.

Equations (1)–(10) complete the necessary formalism of band structure and wave functions. The particular material to be described enters through the two parameters, m^* the effective mass at the conduction-band edge, and $\mathcal{E}_g$ the effective-mass energy gap. m^* will be taken to be temperature independent in the present treatment, although $\mathcal{E}_g$ is variable with temperature according to Ehrenreich,[25]

$$\mathcal{E}_g(T) = \mathcal{E}_g(0) - 3lT\left(\frac{\partial \mathcal{E}_g}{\partial P}\right)_T \Big/ K, \tag{11}$$

where l is the linear coefficient of thermal expansion, $(\partial \mathcal{E}_g/\partial P)_T$ is the rate of change of band gap with pressure, and K is the compressibility. These latter three quantities are assumed temperature independent.

III. BOLTZMANN EQUATION

To determine the low-field drift mobility, one applies a small electric field $\vec{F}$ to the electron population whose equilibrium distribution function is $f_0(k)$ when $\vec{F} = 0$. The spatially uniform and isotropic distribution f_0 undergoes a perturbation due to the electric field so that the distribution in the presence of the field can be written exactly [see the discussion following Eq. (17)] as

$$f(\vec{k}) = f_0(k) + xg(k), \tag{12}$$

where $k = |\vec{k}|$ and x is the cosine of the angle between $\vec{k}$ and $\vec{F}$. The perturbation distribution g will be determined explicitly in Sec. V. The induced drift current is entirely contained in the perturbation distribution.

For a nondegenerate semiconductor, the Boltzmann equation connects g through the scattering mechanisms to the electric field and f_0:

$$0 = -(e/\hbar)\vec{F}\cdot\nabla_k f(\vec{k}) + \int d\vec{k}'[s(\vec{k}', \vec{k})f(\vec{k}') - s(\vec{k}, \vec{k}')f(\vec{k})]. \tag{13}$$

$s(\vec{k}', \vec{k})$ is the probability per unit time that an electron initially in the state characterized by $\vec{k}'$ will make a transition into the state characterized by $\vec{k}$. The differential scattering rate s comprises several scattering mechanisms to be considered in detail in Sec. IV. For the moment, we note that the first integrand corresponds to scattering *into* the differential element $d\vec{k}$ while the second integrand corresponds to scattering *out of* $d\vec{k}$. These terms give rise to the following scattering probability fluxes:

$$\nu_i^{(0)} = \int d\vec{k}'[s(\vec{k}', \vec{k})f_0(k')], \tag{14}$$

$$\nu_i^{(1)} = \int d\vec{k}'[s(\vec{k}', \vec{k})x'g(k')], \tag{15}$$

$$\nu_o^{(0)} = f_0(k)\int d\vec{k}'[s(\vec{k}, \vec{k}')], \tag{16}$$

$$\nu_o^{(1)} = xg(k)\int d\vec{k}'[s(\vec{k}, \vec{k}')], \tag{17}$$

where $k = |\vec{k}|$, $k' = |\vec{k}'|$, and x' is the cosine of the angle between $\vec{k}'$ and $\vec{F}$. A subscript o denotes scattering *out*; i denotes scattering *in*. It turns out that (Sec. IV) $\nu_i^{(0)}$ and $\nu_o^{(0)}$ are isotropic in momentum space, while $\nu_i^{(1)}$ and $\nu_o^{(1)}$ are directly proportional to the cosine of the angle between $\vec{k}$ and $\vec{F}$. This result offers the *a fortiori* proof that Eq. (12) is indeed exact as $\vec{F}$ becomes small.

A spherical harmonic analysis can now be used to separate the Boltzmann equation into the following two equations (see, for example, Baraff[29]). Multiplication of Eq. (13) by unity, the zeroth-order Legendre polynomial, and integration over x yields

$$eF\left(\frac{\partial g(k)}{\partial k} + 2\frac{g(k)}{k}\right)\Big/ 3\hbar = \nu_i^{(0)} - \nu_o^{(0)}, \tag{18}$$

where $F = |\vec{F}|$. Multiplication by the first-order Legendre polynomial x and integration over x provides the remaining equation

$$\frac{eF}{\hbar}\frac{\partial f_0(k)}{\partial k} = \frac{\nu_i^{(1)} - \nu_o^{(1)}}{x}. \tag{19}$$

The right-hand side of Eq. (19) is independent of x since the scattering probability fluxes due to g are proportional to x. The first of these two equations [Eq. (18)] simply guarantees that f_0 is the equilibrium Boltzmann distribution. This follows since g is proportional to $\vec{F}$ so that the left-hand side of Eq. (18) vanishes in first order while $\nu_i^{(0)}$ and $\nu_o^{(0)}$ are of zeroth order in F. The right-hand side of Eq. (18) therefore vanishes for the isotropic distribution f_0 [Eqs. (14) and (16)]. This is the

equilibrium equation and, hence, f_0 follows at once as the Boltzmann distribution.[30]

The perturbation distribution g is contained in Eq. (19) through the scattering probability fluxes $\nu_i^{(1)}$ and $\nu_o^{(1)}$. Both sides of Eq. (19) must be of first order in F. In Sec. IV, the scattering probability fluxes discussed above will be calculated for the various scattering mechanisms of interest here. Those results can then be combined with Eq. (19) to yield an explicit formula for the perturbed distribution.

IV. POLAR-OPTICAL, DEFORMATION-POTENTIAL, AND PIEZOELECTRIC SCATTERING

The scattering probability fluxes of Sec. III can be calculated analytically without approximation from the differential scattering rates including the present band-structure formalism. This fact has been shown previously by Howarth and Sondheimer[24] for parabolic bands and by Ehrenreich[25] for a slightly different form of Kane's[19] band model and for polar-mode scattering. Since the procedure is similar for deformation-potential and piezoelectric scattering, the details of the integration of Eqs. (14)–(17) need not be repeated here. We note that the differential scattering rates denoted by s in Eqs. (14)–(17) consist of sums of differential scattering rates due to (a) polar-mode scattering s_{po}, (b) piezoelectric scattering s_{pe}, and (c) deformation-potential acoustic-mode scattering s_{ac}. These are probably the only important scattering mechanisms in pure nondegenerate polar semiconductors possessing direct gaps for the temperatures indicated in Sec. I.[10]

The inelastic scattering of electrons by polar-optical modes takes place through the coupling of the electron to the associated electric field of the polarization wave.[12,13] The differential scattering rate for this process is found from time-dependent perturbation theory to be proportional to the absolute square of the matrix element of the perturbing potential (Golden Rule No. 2). For the nonparabolic band model of Sec. II, it results that one need only multiply the matrix element determined for parabolic bands by the overlap integral of the wave functions.[25] Matz[28] calculated the overlap integral for Kane's theory, and his result adapted to the present model is given by Eq. (10). The matrix element for scattering by polar modes appears in the literature.[25,31] Substitution into Eq. (16) yields the following result for the scattering-*out* probability flux due to f_0 and only polar-mode scattering:

$$\nu_{o\,po}^{(0)} = f_0(k) \sum_{*} \lambda_o^{*} \frac{m d^{*}}{\hbar k} \times \left(A^{*2} \ln \left| \frac{k^{*}+k}{k^{*}-k} \right| - A^{*} cc^{*} - aca^{*}c^{*} \right), \quad (20)$$

where

$$A^{*} = aa^{*} + (k^{*2}+k^{2})cc^{*}/2k^{*}k . \quad (21)$$

The summation index $*$ takes on the values + and −, corresponding, respectively, to scattering *out* from the differential element $d\vec{k}$ by phonon absorption and by phonon emission. Any quantity superfixed by * is to be evaluated at the energy corresponding to $\vec{k}$ plus or minus (according to the value of *) the energy $\hbar\omega_{po}$ of a longitudinal polar-optical phonon at the center of the first Brillouin zone. Of course, when k corresponds to an energy less than the polar-phonon energy the phonon emission term (*~−) of Eq. (20) is understood to be omitted. d^{*} is the relative density-of-states function, Eq. (6). The a, c, a^{*}, and c^{*} are wave-function coefficients [Eqs. (8) and (9)]. The energy-independent (k-independent) constant λ_o^{*} contains all the temperature dependence of $\nu_{opo}^{(0)}$:

$$\lambda_o^{*} = \frac{e^2\omega_{po}}{4\pi\hbar} \left(\frac{1}{\epsilon_\infty} - \frac{1}{\epsilon_0} \right) \left[N_{po} + \tfrac{1}{2}{}^{*}(-\tfrac{1}{2}) \right] . \quad (22)$$

The high- and low-frequency dielectric constants are ϵ_∞ and ϵ_0. For the small electric fields under present consideration, the phonon population must be at equilibrium so that the average number of phonons N_{po} in the polar vibration mode with which the electron is interacting is given by the Bose distribution:

$$1/N_{po} = \exp(\hbar\omega_{po}/\kappa T) - 1. \quad (23)$$

From Eq. (20), it is evident that $\nu_{opo}^{(0)}$ is isotropic in momentum space and directly proportional to $f_0(k)$. In this case and, in general, for scattering-*out* probability fluxes, one can define the *scattering rate* $S_{opo}(k)$ which depends upon only the magnitude of $\vec{k}$ and which is independent of the distribution function

$$S_{opo} = \nu_{opo}^{(0)}/f_0(k) . \quad (24)$$

The scattering rate has the dimension inverse time.

The scattering-*in* probability flux is

$$\nu_{ipo}^{(0)} = \sum_{*} f_0(k^{*}) \lambda_i^{*} \frac{m d^{*}}{\hbar k} \times \left(A^{*2} \ln \left| \frac{k^{*}+k}{k^{*}-k} \right| - A^{*} cc^{*} - aca^{*}c^{*} \right), \quad (25)$$

where the temperature dependence again appears through λ_i^{*}:

$$\lambda_i^{*} = \frac{e^2\omega_{po}}{4\pi\hbar} \left(\frac{1}{\epsilon_\infty} - \frac{1}{\epsilon_0} \right) \left(N_{po} + \frac{1}{2}{}^{*}\frac{1}{2} \right) . \quad (26)$$

The scattering-*in* and scattering-*out* fluxes [Eqs. (20) and (25)] are identical but (i) the former involves the distribution function at k^{+} and k^{-} as well as at k, and (ii) the phonon occupation number fac-

tors in the constants λ_o^* and λ_i^* are permuted relative to one another. Regarding this latter point, Eqs. (22) and (26) show that scattering *in* from an initial state $\vec{k}' = \vec{k}^+$ to the state $\vec{k}$ is proportional to $N_{po}+1$ (corresponding to phonon emission). However, time reversal of the same process gives scattering *out* from the initial state $\vec{k}$ to the state $\vec{k}' = \vec{k}^+$ as proportional to only N_{po} (phonon absorption). The explanation is simply that time reversal transforms the emission process into an absorption process and vice versa. This explains the difference between λ_i^* and λ_o^* and also the point that the principle of detailed balance suggests, that $S(\vec{k}', \vec{k}) = S(\vec{k}, \vec{k}')$ if and only if the scattering process is elastic.[22,32] It is precisely this point which provides the fundamental difference between scattering terms in the Boltzmann equation for nondegenerate statistics and degenerate statistics. Our results apply only to the former case. The reader can verify from Eqs. (20), (23), and (25) that $\nu_{ipo}^{(0)} = \nu_{opo}^{(0)}$ implies that f_0 is the Boltzmann distribution.

The scattering fluxes due to the perturbation distribution follow from Eqs. (15) and (17). For polar-mode scattering

$$\nu_{opo}^{(1)} = S_{opo}\ xg(k) \tag{27}$$

and

$$\nu_{ipo}^{(1)} = \sum_* xg(k^*)\lambda_i^*\,(md^*/\hbar k) \times \left((k^{*2}+k^2)A^{*2} \ln\left|\frac{k^*+k}{k^*-k}\right| \Big/ 2k^*k - A^{*2} - \tfrac{1}{3}c^2c^{*2} \right) . \tag{28}$$

For an inelastic scattering process, like polar-mode scattering, a scattering-*in* rate evaluated at the energy corresponding to k cannot be defined since the scattering-*in* flux is proportional to the distribution function at this energy plus or minus a phonon energy. In this case, we denote the scattering-*in* rate as S_{ipo}^*,

$$\nu_{ipo}^{(1)} = \sum_*\ xg(k^*)S_{ipo}^* . \tag{29}$$

The superscript * signifies explicitly that S_{ipo}^* is evaluated at k^+ and k^-.

The second of the three types of scattering to be included is deformation-potential scattering by acoustic modes of lattice vibration.[11] This process can be considered elastic.[31] For parabolic bands, deformation-potential scattering is fully randomizing [i.e., $s_{ac}(\vec{k}', \vec{k})$ independent of the angle between $\vec{k}'$ and $\vec{k}$] and the scattering-*in* term of Eq. (15) due to the perturbation distribution g vanishes. However, $s_{ac}(\vec{k}'\,\vec{k})$ is not randomizing for the present band model and the scattering-*in* flux due to g does not vanish. The matrix element, available in the literature,[31] is multiplied by the overlap integral Eq. (10) and Eqs. (14)–(17) are evaluated under the assumption that the acoustic phonon occupation number attains its equipartition value. This assumption sets a low-temperature limit to the validity of the results at about 2 °K:

$$\nu_{oac}^{(0)} = f_0(k)\lambda_{ac}\quad (mdk/\hbar)\tfrac{1}{3}(3a^4+c^4) , \tag{30}$$

where

$$\lambda_{ac} = e^2E_1^2\kappa\, T/\pi\hbar^2\rho u_a^2 , \tag{31}$$

and E_1 is the acoustic deformation potential, ρ is the material density, and u_a is the average speed of sound in the material (see the Appendix). Since deformation-potential scattering is elastic, for arbitrary f_0

$$\nu_{iac}^{(0)} = \nu_{oac}^{(0)} , \tag{32}$$

so that f_0 is unaffected by this scattering mechanism:

$$\nu_{oac}^{(1)} = xg(k)\lambda_{ac}\,(mdk/\hbar)\tfrac{1}{3}(3a^4+c^4) \tag{33}$$

and

$$\nu_{iac}^{(1)} = xg(k)\lambda_{ac}\,(mdk/\hbar)\tfrac{1}{3}(2a^2c^2) . \tag{34}$$

As in the case of polar-mode scattering, the scattering fluxes for deformation-potential scattering are isotropic for f_0 and proportional to x for g, thus guaranteeing the success of the spherical harmonic analysis of Sec. III. Furthermore, both scattering-*in* and scattering-*out* fluxes for this elastic scattering process depend only upon the distribution function evaluated at k. Hence, we can define a scattering rate which includes both fluxes simultaneously:

$$S_{ac} = [\nu_{oac}^{(1)} - \nu_{iac}^{(1)}]/xg(k) . \tag{35}$$

The final scattering mechanism to be considered is piezoelectric scattering.[14,15] Hutson[16,31] has given the matrix element for this process in parabolic bands and we need include the overlap integral [Eq. (10)]. Piezoelectric coupling occurs in appreciable magnitude only to the longitudinal electric fields.[17] The strength of the coupling is proportional to the piezoelectric constant e_{14} which, incidentally, is larger in III-V compounds than in the more ionic cubic II-VI compounds. Arlt and Quadflieg[33] have measured e_{14} for a variety of materials and have proposed that piezoelectricity is due to the mechanisms of (a) ionic polarization, (b) change in ionicity, and (c) electronic polarization. Recently, Phillips and Van Vechten[34] presented theoretical arguments to explain the change in algebraic sign of e_{14} as one goes from III-V compounds to II-VI compounds. Their results suggest that b above, which accounts for the strain-induced flow of covalent charge between the zinc-blende sublattices, may be the dominant source of piezoelectricity in many of the III-V compounds.

At this point, it is worth remarking that one cannot calculate a scattering-*out* rate for piezoelec-

tric scattering since this quantity is (mathematically) singular due to the predominance of small-angle scattering. The scattering probability flux $\nu_{ope}^{(0)}$ does not exist as a finite number. There is, however, no need for $\nu_{ope}^{(0)}$ by itself. The meaningful quantity is the *difference* between scattering *in* and scattering *out*. This quantity does exist in a well-behaved manner for piezoelectric scattering,

$$\nu_{ope}^{(0)} - \nu_{ipe}^{(0)} = 0 \quad , \tag{36}$$

since piezoelectric scattering is elastic [see Eq. (32)], and

$$\nu_{ope}^{(1)} - \nu_{ipe}^{(1)} = xg(k)\lambda_{pe}(md/\hbar k)\tfrac{1}{3}(3a^4 + c^4) \quad , \tag{37}$$

where

$$\lambda_{pe} = e^2 e_{14}^2 \kappa T / 2\pi \epsilon_0^2 \hbar^2 \rho u_p^2 \tag{38}$$

and ϵ_0 is the low-frequency dielectric constant. The speed of sound u_p includes the effect of transverse and longitudinal modes and is discussed in the Appendix. The law of equipartition assumption[32] again limits the application of Eq. (37) to temperatures greater than about 2 °K.

Note that Eqs. (33) and (37) are quite similar except that deformation-potential scattering is directly proportional to the crystal momentum k of the electron whereas piezoelectric scattering is inversely proportional to k. It follows that piezoelectric scattering must dominate deformation-potential scattering below a certain temperature T_{co}. This crossover temperature, taking $a = 1$, occurs at

$$T_{co} \approx \hbar^2 e_{14}^2 / 4\kappa m \epsilon_0^2 E_1^2 \approx 150 \text{ °K} \quad . \tag{39}$$

T_{co} does not vary greatly over the direct-gap III-V semiconductors. In fact, polar-mode scattering dominates at 150 °K where piezoelectric scattering effects on the mobility become just noticeable (~10%). Below about 60 °K in GaAs, piezoelectric scattering is the dominant mobility-limiting mechanism. The conclusion is that deformation-potential scattering is never dominant in these semiconductors. Finally, analogous to Eq. (35) is a scattering rate for piezoelectric scattering which includes scattering *in* and scattering *out*:

$$S_{pe} = [\nu_{ope}^{(1)} - \nu_{ipe}^{(1)}] / xg(k) \quad . \tag{40}$$

V. PERTURBATION DISTRIBUTION FUNCTION

Section IV provides explicit formulas for the scattering terms of the Boltzmann equation including polar-mode, deformation-potential, and piezoelectric scattering. These results are to be combined in the present section with the results of Sec. III, the spherical harmonic analysis of the Boltzmann equation. From Eqs. (19), (27), (29), (35), and (40) directly follows the formula for the perturbation distribution g.

First, we combine the scattering rates for all three scattering mechanisms into the total scattering rate S_0:

$$S_0 = S_{opo} + S_{ac} + S_{pe} \quad . \tag{41}$$

Note that S_0 contains all three scattering-*out* rates as well as the scattering-*in* rates for elastic processes as shown in Sec. IV. The only scattering-*in* rate remaining is due to inelastic polar-mode scattering. Combining these results leaves

$$g(k) = \frac{S_{ipo}^{+} g(k^{+}) + S_{ipo}^{-}(k^{-}) - eFf_0(k)'/\hbar}{S_0} \quad , \tag{42}$$

where $f_0(k)' = \partial f_0 / \partial k$ and k^{+} and k^{-} are as discussed after Eq. (21). Equation (42) is a linear finite difference equation similar to that found previously.[24,25] However, we will not, as previously, apply variational methods to the solution of Eq. (42).

The perturbation distribution can be easily and rapidly found by numerical iteration. We choose the zeroth-iteration solution $g_0(k) = 0$ for all k. Then

$$g_1(k) = -\frac{eF}{\hbar S_0} \frac{\partial f_0}{\partial k} \tag{43}$$

and, in general,

$$g_{i+1} = (S_{ipo}^{+} g_i^{+} + S_{ipo}^{-} g_i^{-} + F_0')/S_0 \quad , \tag{44}$$

where $g_i^{*} = g_i(k^{*})$ and $F_0' = -eFf_0'/\hbar$. The first iteration [Eq. (43)] gives the usual result for a relaxation approximation,[22] that g is proportional to the slope of f_0. The solution g_1 simply ignores scattering *in*, which is justifiable at temperatures well below the Debye temperature of the polar-optical phonons. This is so because scattering *in* by phonon emission is possible for only the very few electrons which would have a phonon quantum of energy. Scattering *in* by the remaining process, phonon absorption, is also extremely weak since at low temperatures very few vibrational modes are occupied by a phonon [see Eq. (23)]. For example, in GaAs the polar-phonon Debye temperature is 420 °K (see Sec. VI) and the use of g_1 to calculate the mobility at a lattice temperature of 77 °K leads to an underestimate of the mobility by only 6.5%. At 300 °K there is a noticeable amount of scattering *in*, and the use of g_1 leads to an underestimate of the true mobility by 33%. Three iterations according to Eq. (44) at 300 °K give the answer correct to 10%. (In practice, the results to be presented later are calculated to less than 1% error.) The relaxation approximation [Eq. (43)] yields Frohlich's low-temperature expression for polar-mode-limited mobility when deformation-potential and piezoelectric scattering are omitted.[12]

The above discussion is illustrated in detail by Figs. 1 and 2, drawn for GaAs. In Fig. 1 for $T = 77\,^{\circ}\mathrm{K}$, the total scattering-*out* rate S_0 is plotted as the dashed curve. S_0 is large for small momenta due to piezoelectric scattering. The fairly constant value of S_0 over most of the figure represents scattering *out* by optical phonon absorption. Deformation-potential scattering is insignificant. The Boltzmann distribution f_0 indicates the location of most electrons in the figure. The perturbation distribution g is calculated from Eq. (44) and compared in the figure to $g_1 \sim -f_0'/S_0$ from Eq. (43). The agreement between g and g_1 is fairly good, reflecting the 6.5% error in mobility from g_1 mentioned earlier.

Figure 2 is identical to Fig. 1 except that the lattice temperature is now 300 °K so that an appreciable number of electrons carry a phonon equivalent quantum of energy (~420 °K). The total scattering rate S_0 resembles that of Fig. 1 at low momenta. When $\hbar k \geq 1.2$, the electrons can emit phonons and S_0 is enhanced by the phonon emission process. f_0 again is the Boltzmann distribution, and the actual perturbation g is compared to that obtained from a relaxation approximation g_1. The disagreement is now considerable due to the scattering-*in* terms of Eq. (44).

It can be noted at this point that the present method of solution for g preserves the same advantages as variational approaches without, however, the need for excessive mathematical detail. The approximate expression g_1 is always less than g because all scattering-*in* quantities are nonnegative for all momenta. It follows that $g_i < g$

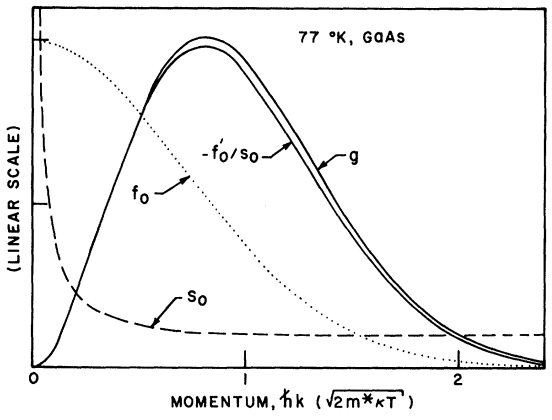

FIG. 1. Perturbation electron distribution function $g(k)$ induced by a small electric field. The equilibrium Boltzmann distribution is f_0. The total scattering-out rate is S_0. $-f_0'/S_0$ represents the relaxation approximation to the true perturbation distribution $g(k)$ and is rather accurate for this case of GaAs at 77 °K.

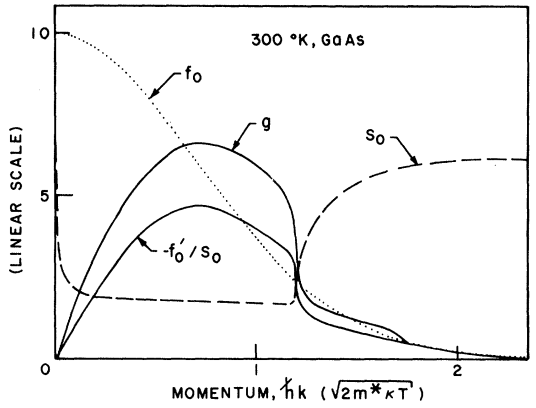

FIG. 2. Same as Fig. 1 except the GaAs lattice temperature $T = 300\,^{\circ}\mathrm{K}$. The relaxation approximation $(-f_0'/S_0)$ to the true perturbation distribution $g(k)$ fails seriously (notice the large disparity between the $-f_0'/S_0$ and g curves) due to considerable scattering in by phonon emission.

(treating g as positive) for all i where g satisfies Eq. (42). Therefore, as in the variational approach, the convergence of g_i to g, or similarly the mobility, forms a monotone sequence, i.e., any particular g_i is a lower limit on g. In addition, the convergence of the sequence $\{g_i\}$ is rapid and nearly exponential so that the remaining error after the $i+1$ iteration is approximately equal to the difference between the i and $i+1$ iteration.

Before explicitly relating $g(k)$ to the mobility (see Sec. VI), we justify the inclusion of (a) Kane's model[19] for the conduction band, and (b) piezoelectric scattering.[16,17] Regarding the importance of Kane's model[19] of the conduction-band structure and wave functions, Fig. 3 has been plotted to compare electron mobility with Kane's model to a parabolic band. For parabolic bands, a of Eq. (7) equals unity, $c = 0$, and the energy Eq. (3) becomes $\mathcal{E} = \hbar^2 k^2/2m^*$. The mobilities for parabolic bands in GaAs (with the largest energy gap of the present materials) and InSb (the smallest gap) are shown as dashed curves. The correct mobilities are plotted as solid curves. Evidently, the InSb conduction band is considerably nonparabolic, leading to 50% differences between mobility for parabolic and nonparabolic bands.[26] In the wide-gap material GaAs, the valence–conduction-band interaction must be relatively small so that nonparabolicity affects the mobility by only about 10%.

The dominance of piezoelectric scattering toward limiting the drift mobility at low temperatures can be appreciated from the comparison in Fig. 4. Piezoelectric scattering has been omitted

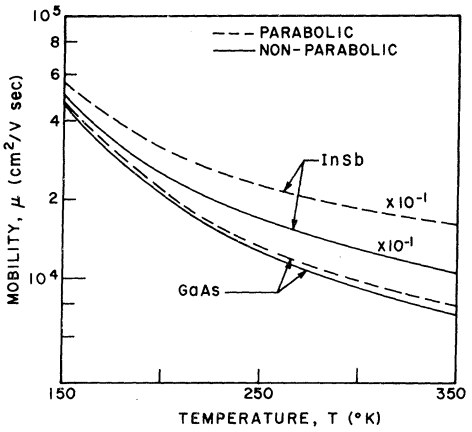

FIG. 3. Comparison of electron drift mobility in GaAs and InSb for parabolic and nonparabolic conduction bands. The nonparabolic band model more accurately represents the actual physical situation.

in the calculation of mobility plotted as dashed curves in GaAs and InSb while the correct mobility is represented by the solid curves. InSb has the lowest polar-phonon Debye temperature (278 °K) of the five materials being considered so that polar-mode scattering dominates to lower temperatures (~40 °K) than in the remaining materials. On the other hand, the polar-phonon Debye temperature is relatively higher in GaAs (being 420 °K) so that the average phonon occupation number [Eq. (23)] decreases rapidly with temperature. In this case, polar-mode scattering becomes weaker than piezoelectric scattering at lattice temperatures below 60 °K. For temperatures as high as 150 °K in GaAs, piezoelectric scattering causes a decrement in mobility of 11%.

VI. RESULTS

The mobility can be found immediately from Eq. (44) and the following equations. First of all, the distribution function must be normalized so that

$$1 = \int f_0 d\vec{k} \quad . \tag{45}$$

Now the mobility is

$$\mu = \tfrac{4}{3}\pi \cdot (\hbar/m) \int [g(k)/Fd] k^3 dk \quad , \tag{46}$$

where d is the relative density-of-states function [Eq. (6)], which in the present context allows that the group velocity of the electron wave function no longer equals the phase velocity. Although the mobility equation (46) contains the electric field magnitude F, μ is independent of F since g/F is independent of F by Eq. (42), i.e., Ohm's law is valid at low electric fields.

There are 12 material parameters required for calculating the electron drift mobility according to the model of the previous sections. The necessary quantities are listed in Table I. The most accurate data available are probably those for GaAs. We will discuss in detail only the data relevant to GaAs as an illustration of how Table I has evolved from a wide selection of experimental evidence (see, for example, Refs. 35–37).

The electron effective mass at the conduction-band edge in GaAs has been measured and reviewed by Chamberlain and Stradling,[38] whose discussion indicates $m^* = 0.0655m$ (assumed temperature independent for the present work). For the energy-gap parameters [Eq. (11)] $\mathcal{E}_g(0)$ is taken as the *thermal* gap at zero temperature[35] while the linear coefficient of thermal expansion[36] l is assigned an average temperature-independent value. The compressibility K also is assumed temperature independent and is calculated from the elastic constants[36] c_{ij} through the relation $K = 3/(c_{11} + 2c_{12})$. These various assumptions of temperature independence do not effect errors in mobility of more than a few percent. Polar-mode scattering, depending as it does on the small difference between the relatively large high- and low-frequency dielectric constants [Eqs. (22) and (26)], is sensitive to small errors in ϵ_0 and ϵ_∞. However, experimental values for the product $\epsilon_0\epsilon_\infty$ are well established.[35–37] For this reason, ϵ_0 and ϵ_∞ have been determined from $\epsilon_0\epsilon_\infty$ and $\epsilon_0/\epsilon_\infty = (\nu_0/\nu_1)^2$, where ν_0 and ν_1 are the respective lon-

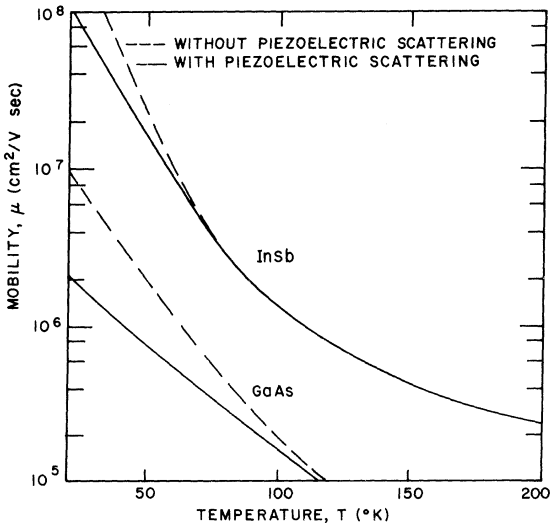

FIG. 4. Electron drift mobility in GaAs and InSb including (a) polar-mode, deformation-potential accustic-mode, and piezoelectric scattering (solid lines), and (b) neglecting piezoelectric scattering.

TABLE I. Material parameters.

Quantity	GaAs	GaSb	InP	InAs	InSb
Effective mass m^*/m	0.0655	0.047	0.067	0.022	0.013
Zero-temperature energy gap $\mathcal{E}_g(0)$ (eV)	1.58	0.80	1.48	0.46	0.265
Energy-gap temperature coefficient $3l(\partial \mathcal{E}_g/\partial P)_T/K(10^{-4}\,\mathrm{eV}/^\circ\mathrm{K})$	1.20	1.16	0.50	0.79	1.12
Low-frequency dielectric constant ϵ_0	12.90	15.00	12.30	14.55	18.70
High-frequency dielectric constant ϵ_∞	10.92	13.80	9.56	11.78	16.76
Polar-phonon Debye temperature T_{po} (°K)	420	346	501	350	278
Material density ρ (g/cm^3)	5.36	5.66	4.83	5.71	5.82
Sound speed u_a (km/sec)	5.24	4.36	5.16	4.28	3.80
Acoustic deformation potential E_1 (eV)	7.0	6.7	6.5	4.9	7.2
Piezoelectric constant $e_{14}(C/m^2)$	0.160	0.126	0.035	0.045	0.071
Sound speed u_p (km/sec)	4.03	3.35	3.85	3.17	2.78

gitudinal and transverse optical phonon frequencies[39] at the center of the first Brillouin zone. ϵ_0 and ϵ_∞ from direct measurements[40–42] (respectively, 13.0 and 10.9) compare favorably to ϵ_0 and ϵ_∞ derived in the above way (respectively, 12.90 and 10.92). The ratio $\epsilon_0/\epsilon_\infty$ does not appear to be significantly temperature dependent.[43] The polar-phonon Debye temperature[39] is $T_{po} = \hbar\omega_{po}/\kappa$. The density ρ follows from the lattice constant[36] and the sound speeds u_a and u_p assume average values. E_1 is calculated as suggested by Ehrenreich[23] and does not include dependences of the valence-band position upon strain. Although E_1 may thus be in considerable error, the mobility is fairly unaffected because deformation-potential scattering is quite weak. The piezoelectric constant e_{14}, except for InP and InAs, is probably more accurate than the 10–20% stated by Arlt and Quadflieg[33] in view of the good agreement with theory.[34] These considerations lead cumulatively to the estimated errors in mobility stated in Sec. I.

The electron drift mobilities versus temperature of GaAs, GaSb, and InP are presented in Fig. 5. At higher temperatures, there is some transfer of electrons into higher-lying valleys near the edges of the first Brillouin zone.[37] Due to this effect, the results of Fig. 5 are estimated to be accurate to 10% only below 500 °K in GaAs, 170 °K in GaSb, and 600 °K in InP. The unreliable portions of the curves above these temperatures in Fig. 5 are dotted. Since mobilities are frequently quoted at 300 and at 77 °K, the mobility at these temperatures is tabulated in Table II.

The mobilities versus temperature for InAs and InSb appear in Fig. 6, where again the curves at higher temperatures are dotted. These regions indicate the failure of the present model for these

TABLE II. Calculated electron drift mobility ($cm^2/V\,sec$).

Temperature (°K)	GaAs	GaSb	InP	InAs	InSb
300	8920	•••	6860	31 800	129 000
77	2.96×10^5	5.76×10^5	5.86×10^5	1.50×10^4	3.08×10^6

narrow energy-gap materials because of degeneracy.[26] The density of thermally stimulated carriers is considerable in InSb at room temperature[35] ($n=2\times10^{16}$ cm^{-3}). Above 350 °K, transport in InSb must include Fermi statistics. InAs should be reasonably nondegenerate up to 600 °K.

Experimental data from Hall measurements at high[44] and low[45] temperatures on GaAs provide essential confirmation of the present results. In Fig. 7 the electron drift mobility in GaAs from the present work is plotted as a solid curve. The solid data points for temperatures 50–300 °K are derived from Hall mobility measurements published by Hicks and Manley.[45] High-temperature ($\geq$ 300 °K) Hall data by Chang[44] are plotted as triangular points in Fig. 7. Since polar-mode scattering dominates in both these GaAs samples above 100 °K, the conversion from Hall mobility to drift mobility can be, and has been, made in the figure from Ehrenreich's[26] results on InSb. In any case, the correction on this account does not exceed 20% and is, therefore, hardly noticeable on the scale of Fig. 7. Undoubtedly the experimentally derived mobility below 80 °K is limited by impurity scattering[31] which is not of interest here. The high-temperature data fall somewhat farther below the predicted curve for temperatures exceeding 450 °K than is to be expected. This difference remains unresolved. The explanation may reside in a revised estimate of the energy separation between the (000) and ⟨100⟩ valleys (taken to be 0.36 eV[23]). Temperature dependences of the effective mass[25] and dielectric constants[41,46,47] have the wrong trends for lowering the mobility with increasing temperature.

In the region of room temperature, the experimental data bracket the theoretical curve which, incidentally, derives from a calculation entirely devoid of adjustable parameters. This fact in

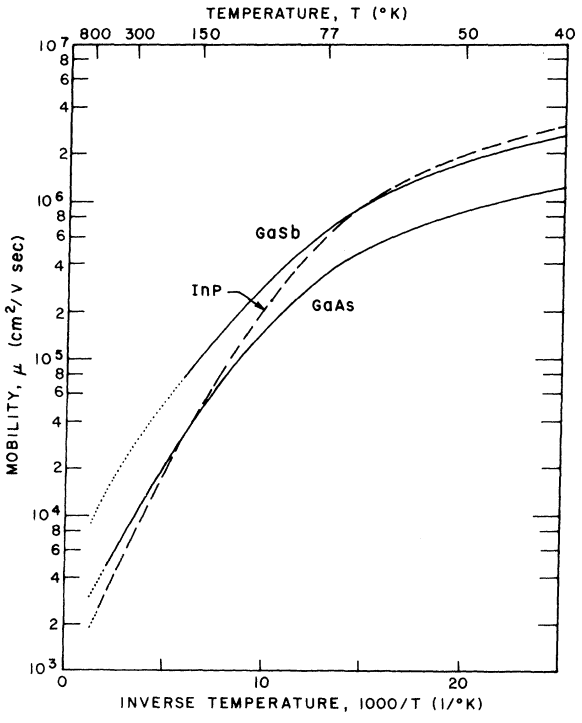

FIG. 5. Electron drift mobility in GaAs, GaSb, and InP. The dotted portions of the curves at higher temperatures are not reliable (see text) because of electron transport in higher-lying conduction-band minima.

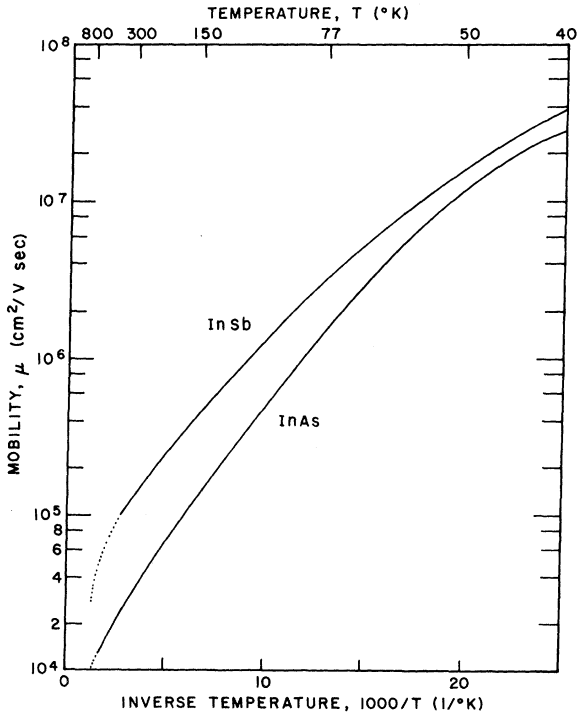

FIG. 6. Electron drift mobility in InAs and InSb. The dotted portions of the curves at higher temperatures are not reliable (see text) because of degeneracy.

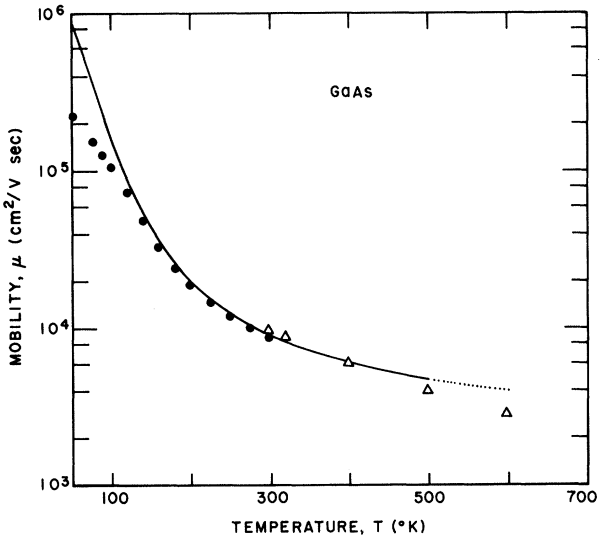

FIG. 7. Comparison between electron drift mobility in GaAs calculated with parameters listed in Table I (solid curve) and drift mobility derived from experimental Hall mobility data via thoeretical Hall factor correction (solid points from Hicks and Manley[45]; triangular points from Chang[44]).

addition to the substantial agreement over the 120–500 °K region suggests a satisfactory verification of the present model for pure material.

Note added in proof. The present technique for calculating drift mobilities has been successfully extended to include ionized impurity scattering and equivalent intervalley scattering appropriate to *indirect-* as well as direct-gap semiconductors. Electron-hole scattering lowers the room-temperature mobility in InSb to 70 400 cm^2/V sec as opposed to the value shown in Table II. Result for impure materials and for indirect-gap materials will be published in the near future.

ACKNOWLEDGMENTS

D. F. Manley[45] was most helpful in providing detailed mobility data on GaAs at low temperatures. J. Barrera and D. M. Chang[44] were kind enough to discuss their high-temperature mobility results prior to publication of same. The author has benefited from many discussions with W. Fawcett and J. G. Ruch.

APPENDIX

The spherically averaged elastic stiffness constants which yield u_a in Eq. (31) and u_p in Eq. (38) have been calculated by Zook.[48] For deformation-potential acoustic-mode scattering in zinc-blende crystals,

$$\rho u_a^2 = c_l \ , \tag{A1}$$

where[48] $c_l = \frac{1}{5}(3c_{11} + 2c_{12} + 4c_{44})$ (A2)

and the elastics constants[36] are c_{ij}.

For piezoelectric scattering by the longitudinal electric fields of longitudinal and transverse acoustic modes,

$$1/\rho u_p^2 = \tfrac{1}{35}(12/c_l + 16/c_t) \ , \tag{A3}$$

where[48] $c_t = \frac{1}{5}(c_{11} - c_{12} + 3c_{44})$. (A4)

[1]E. J. Huibregtse, IBM J. Res. Develop. 13, 485 (1969).
[2]J. C. Phillips J. Phys. Soc. Japan Suppl. 21, 3 (1966).
[3]L. F. Eastman, IEEE Trans. Electron Devices LD-14, 460 (1967).
[4]H. C. Casey and F. A. Trumbore, Mater. Sci. Eng. 6, 69 (1970).
[5]W. Fawcett and J. G. Ruch, Appl. Phys. Letters 15, 368 (1969).
[6]H. D. Rees, J. Phys. Chem. Solids 30, 643 (1969).
[7]J. B. Gunn, IBM J. Res. Develop. 8, 141 (1964).
[8]J. A. Copeland, J. Appl. Phys. 38, 3096 (1967).
[9]F. J. Blatt, in *Solid State Physics*, edited by F. Seitz and D. Turnbull (Academic, New York, 1957), Vol. 4.
[10]H. Ehrenreich, J. Appl. Phys. Suppl. 32, 2155 (1961).
[11]J. Bardeen and W. Shockley, Phys. Rev. 80, 72 (1950).
[12]H. Frohlich, Advan. Phys. 3, 325 (1954).
[13]H. B. Callen, Phys. Rev. 76, 1394 (1949).
[14]H. J. G. Meijer and D. Polder, Physica 19, 255 (1953).
[15]W. A. Harrison, Phys. Rev. 101, 903 (1956).
[16]A. R. Hutson, J. Appl. Phys. Suppl. 32, 2287 (1961).
[17]A. R. Hutson and D. L. White, J. Appl. Phys. 33, 40 (1962).
[18]Matthiessen's rule states that the total resistivity equals the sum of the component resistivities due to each scattering mechanism acting independently. This rule is not generally reliable in the present problem (see Ref. 9, p. 330).
[19]E. O. Kane, J. Phys. Chem. Solids 1, 249 (1957).
[20]J. C. Slater, Rev. Mod. Phys. 6, 209 (1934).
[21]M. Kohler, Z. Physik 125, 679 (1949).
[22]J. M. Ziman, *Electrons and Phonons* (Oxford U. P., London, 1967).
[23]H. Ehrenreich, Phys. Rev. 120, 1951 (1960).
[24]D. J. Howarth and E. H. Sondheimer, Proc. Roy. Soc. (London) A219, 53 (1953).
[25]H. Ehrenreich, J. Phys. Chem. Solids 2, 131 (1957).
[26]H. Ehrenreich, J. Phys. Chem. Solids 9, 129 (1959).
[27]N. N. Grigor'ev, I. M. Dykman, and P. M. Tomchuk, Fiz. Tverd. Tela 10, 1058 (1968) [Soviet Phys. Solid State 10, 837 (1968)].
[28]D. Matz, Phys. Rev. 168, 843 (1968).
[29]G. A. Baraff, Phys. Rev. 133, A26 (1964).
[30]One actually needs to include some inelastic scat-

tering with an equilibrium phonon distribution to prove f_0 Maxwellian. This is a natural consequence of the fact that elastic scattering alone cannot affect the isotropic part of the distribution.

[31]E. M. Conwell, *High Field Transport in Semiconductors* (Academic, New York, 1967).

[32]R. E. Peierls, *Quantum Theory of Solids* (Oxford U. P., London, 1964).

[33]G. Arlt and P. Quadflieg, Phys. Status Solidi 25, 323 (1968).

[34]J. C. Phillips and J. A. Van Vechten, Phys. Rev. Letters 23, 1115 (1969).

[35]C. Hilsum and A. C. Rose-Innes, *Semiconducting III-V Compounds* (Pergamon, New York, 1961).

[36]O. Madelung, *Physics of III-V Compounds* (Wiley, New York, 1964).

[37]*Semiconductors and Semimetals*, edited by R. K. Willardson and A. C. Beer (Academic, New York, 1966).

[38]J. M. Chamberlain and R. A. Stradling, Solid State Commun. 7, 1275 (1969).

[39]M. Hass, in *Semiconductors and Semimetals*, edited by R. K. Willardson and A. C. Beer (Academic, New York, 1967), Vol. III.

[40]K. G. Hambleton, C. Hilsum, and B. R. Holeman, Proc. Phys. Soc. (London) 77, 1147 (1961).

[41]T. Lu, G. H. Glover, and K. S. Champlin, Appl. Phys. Letters 13, 404 (1968).

[42]C. J. Johnson, G. H. Sherman, and R. Weil, Appl. Opt. 8, 1667 (1969).

[43]R. K. Chang, J. M. Ralston, and D. E. Keating, in *Proceedings of the International Conference on Light Scattering Spectra of Solids* (Springer, New York, 1969).

[44]D. M. Chang (private communication from J. Barrera).

[45]H. G. B. Hicks and D. F. Manley, Solid State Commun. 7, 1463 (1969).

[46]D. T. F. Marple, J. Appl. Phys. 35, 1241 (1964).

[47]S. Baron and D. L. Rode (unpublished) have measured $(1/\epsilon_\infty)\,\partial\epsilon_\infty/\partial T = 1.3\times10^{-4}/°\mathrm{K}$ for a photon energy of 0.37 eV which nearly equals the $(1/\epsilon_0)\,\partial\epsilon_0/\partial T = 1.0\times10^{-4}/°\mathrm{K}$ reported in Ref. 41.

[48]J. D. Zook, Phys. Rev. 136, A869 (1964).

PHYSICAL REVIEW B VOLUME 2, NUMBER 4 15 AUGUST 1970

Properties of Electrons in Semiconductor Inversion Layers with Many Occupied Electric Subbands. I. Screening and Impurity Scattering

Eric D. Siggia* and P. C. Kwok

IBM Thomas J. Watson Research Center, Yorktown Heights, New York 10598

(Received 23 December 1969)

Recently, experiments on the properties of electrons in semiconductor inversion layers have been carried out at very high electric fields. These fields correspond to electronic occupation of more than one of the discrete electric subbands created for motion perpendicular to the surface. Previous theoretical investigation on the problem was limited to the case when one subband is populated. In this paper we examine the more general case of having many subbands occupied, studying in detail two particular properties of the system. The first is the electron screening of an external potential described very conveniently by a matrix dielectric function. The second is the scattering of electrons by screened charged impurities and its contribution to the surface conductivity.

I. INTRODUCTION

When a sufficiently strong electric field is applied across the interface of an insulator and a p-type semiconductor, an n-type inversion layer is formed in the semiconductor localized near the surface. This occurs when the conduction-band edge is bent near or below the Fermi level in the bulk. The shape of the bending is determined by the self-consistent electrostatic potential arising mainly from the electrons in the inversion layer. The self-consistent potential produces discrete levels for motion in the direction perpendicular to the surface. These levels are known as electric subbands. The motions of the electrons in the direction parallel to the surface remain essentially Bloch-like. As the field increases, the energies of the discrete levels are lowered and at the same time their separations become larger. Eventually these subbands drop below the bulk Fermi surface in succession. In this paper we shall be concerned entirely with the properties of the inversion layers at high enough field such that several of the discrete subbands are occupied and the population in the continuum levels is negligible.[1]

Stern and Howard[2] represented the first system-